SCIENTIFIC REPORTS

OPEN

Highly selective and sensitive macrocycle-based dinuclear foldamer for fluorometric and colorimetric sensing of citrate in water

Received: 1 September 2017
Accepted: 8 December 2017
Published online: 10 January 2018

Md Mhahabubur Rhaman[1], Mohammad H. Hasan[2], Azmain Alamgir[1], Lihua Xu[3], Douglas R. Powell[4], Bryan M. Wong[3], Ritesh Tandon[2] & Md. Alamgir Hossain[1]

The selective detection of citrate anions is essential for various biological functions in living systems. A quantitative assessment of citrate is required for the diagnosis of various diseases in the human body; however, it is extremely challenging to develop efficient fluorescence and color-detecting molecular probes for sensing citrate in water. Herein, we report a macrocycle-based dinuclear foldamer (1) assembled with eosin Y (EY) that has been studied for anion binding by fluorescence and colorimetric techniques in water at neutral pH. Results from the fluorescence titrations reveal that the 1·EY ensemble strongly binds citrate anions, showing remarkable selectivity over a wide range of inorganic and carboxylate anions. The addition of citrate anions to the 1·EY adduct led to a large fluorescence enhancement, displaying a detectable color change under both visible and UV light in water up to 2 μmol. The biocompatibility of 1·EY as an intracellular carrier in a biological system was evaluated on primary human foreskin fibroblast (HF) cells, showing an excellent cell viability. The strong binding properties of the ensemble allow it to be used as a highly sensitive, detective probe for biologically relevant citrate anions in various applications.

The selective sensing of anions is an important area in supramolecular chemistry due to their significant roles in diverse chemical, biological, medicinal, and environmental science applications[1]. In particular, there is a growing interest in designing artificial receptors that can selectively recognize anions and act as sensors[2,3]. A wide variety of host receptors have been reported that can effectively bind anions in solution and in the solid states, exhibiting selectivity toward certain anions[4–7]. In this regard, carboxylates are of great interest due to their important roles in chemistry and biology[8–10]. Several multi-carboxylates including citrate, succinate, malate, and fumarate are critical chemical species in living cells that are involved in the *Krebs cycle* to generate energy used by aerobic cells in humans[11]. Other carboxylates such as oxalate, tartrate, and glutamate are produced as intermediates during the process of cellular metabolism[12,13]. An oxalate anion is naturally present in several foods and serves as a nutrient in the human body; however, an excess consumption of oxalate is associated with the development of kidney stones[14]. In particular, citrate is widely used in the pharmaceutical industry as an anticoagulant to stop blood clotting[15] and in the food industry as a preservative across the broad spectrum of food and beverage products[16]. Since citrate in urine is considered to inhibit the crystallization of calcium salt, a low amount of citrate in urine is associated with the increased risk of urological diseases such as *nephrolithiasis* and *hypocitraturia*[17,18]. Therefore, citrate is quantitatively determined by a number of instrumental methods, such as gas chromatography, high-performance liquid chromatography, capillary electrophoresis, and enzyme assay[19–21] that are limited

[1]Department of Chemistry and Biochemistry, Jackson State University, Jackson, MS, 39217, USA. [2]Department of Microbiology and Immunology, University of Mississippi Medical Center, Jackson, MS, 39216, USA. [3]Department of Chemical & Environmental Engineering and Materials Science & Engineering Program, University of California-Riverside, Riverside, CA, 92521, USA. [4]Department of Chemistry and Biochemistry, University of Oklahoma, Norman, OK, 73019, USA. Correspondence and requests for materials should be addressed to B.M.W. (email: bryan.wong@ucr.edu) or R.T. (email: rtandon@umc.edu) or M.A.H. (email: alamgir.hossain@jsums.edu)

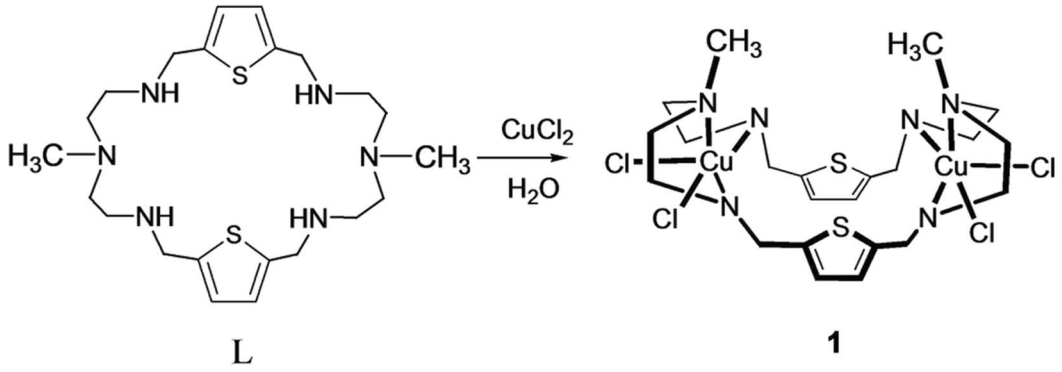

Figure 1. Macrocycle **L** and its dinuclear copper complex **1**.

to *in vitro* samples. In this regard, molecular sensors, which are based on non-covalent interactions, can provide real-time information of intracellular chemistry[22]. As a result, the development of simple and color-detecting molecular devices to identify citrate is highly desirable, particularly in water at neutral pH.

Many artificial chemosensors have been developed for the detection of citrates in recent years[23–26]. For example, Anslyn and co-workers developed a *tris*-guanidinium-based chemosensor that effectively binds citrate in aqueous solution[26]. Schmuck and Schwegmann synthesized a tripodal guanidininocarbonyl pyrrole as a citrate binding host[27]. Stang, Chi, and coworkers reported ruthenium-based tetranuclear metalla-bowls that bind with multi-carboxylate anions such as oxalate, tartrate, and citrate[28]. The majority of reported receptors are designed based on a covalently attached signaling unit (chromophore or fluorophore), that are primarily based on electrostatic or hydrogen bonding interactions. Recently, dinuclear metal complexes were shown as excellent hosts that recognize certain anions through metal-ligand interactions[29–42]. Nelson and coworkers reported a dicopper(II) complex of a *m*-xylyl-based cryptand for N_3^- or NCS^-[31]. Fabbrizzi and coworkers studied a dicopper(II) complex of a furan-based cryptand for halides[32], and a dinuclear copper(II) complex of an expanded cryptand for nucleoside monophosphates[33]. Delgado and coworkers described dinuclear copper(II) complexes for binding of oxalate and succinate anions[35,36]. To the best of our knowledge, dinuclear metal compounds, however, have not been exploited for citrate binding so far. Herein, we report a macrocycle-based dinuclear copper(II) complex (**1**) containing a folded cavity that selectively binds citrate over a wide range of anions in pure water at neutral pH, providing a sharp color change in the presence of an external dye (eosin Y).

Results and Discussion

Design and Synthesis. The design of the macrocycle-based dimetallic complex **1** was based on a concept developed by Lehn, who reported a *bis*tren-based copper cryptate termed as a "cascade complex" for bridging of an anion between the two metal centers[43]. This concept was successfully applied to other *bis*tren-cryptands[31–34] and to *bis*dien-based macrocycles[36–42,44] incorporated with two transition metal ions (e.g. Cu^{II}). In this study, we have chosen a simple methyl-substituted hexaaza-macrocycle **L** (Fig. 1) that was synthesized from the high dilution condensation reactions of an equimolar ratio of *N*-methyl-2,2′-diaminodiethylamine and 2,5-thiophenedicarbaldehyde followed by the reduction with $NaBH_4$ in methanol[45]. The dinuclear copper(II) complex $[Cu_2^{II}(\mathbf{L})Cl_4]$ (**1**) was prepared by adding two equiv. of copper(II) chloride to **L** in a water-methanol mixture. The blue micro-crystals that formed immediately were filtered and recrystallized from slow evaporation of a water solution, yielding X-ray quality crystals. Numerous attempts to grow crystals of anion complexes were unsuccessful. Through the analysis from the indicator displacement assay (IDA), we have shown that the receptor binds the citrate anion selectively over a wide range of dicarboxylates and inorganic anions, forming a 1:1 stoichiometric complex. High level DFT calculations further support the formation of the citrate complex with the receptor through metal-ligand coordination.

Crystal Structure Analysis. The X-ray analysis of the copper complex reveals that it crystallizes as $[Cu_2^{II}(\mathbf{L})Cl_3]_n{\cdot}nCl{\cdot}xH_2O$, (**1′**) in the orthorhombic space group *Amm2* with two copper(II) ions at both N_3 sites. Each copper ion is coordinated with three macrocyclic nitrogens and two chlorides forming a square pyramidal geometry. As shown in Fig. 2a, the macrocycle is folded to form a boat-like shape with an empty cavity where the Cu···Cu distance is 6.3071(11) Å. A similar structure was observed previously for $[Cu_2^{II}(\mathbf{L})Br_4]{\cdot}2H_2O$, with a Cu···Cu distance of 6.243 Å[40]. Each coordinating copper contains one equatorial and one axial chloride. The $Cu-Cl_{equatorial}$ distance is 2.2416(12) Å for Cu1−Cl1, while the $Cu-Cl_{axial}$ distance is 2.7191(5) Å for Cu1−Cl2. The longer distance in $Cu-Cl_{axial}$ is due to a characteristic Jahn-Teller distortion[39]. The Cu−N distances range from 2.022(2) to 2.034(4) Å. The bond angle of N4−Cu1−N1 (or $N4^i$−Cu1−N1) is 84.85(7)°, while that of N4−Cu1−Cl1 (or $N4^i$−Cu1−Cl1) is 96.65(7), which are almost close to 90° required for a perfect square pyramidal geometry. The chloride Cl3 (not shown in Fig. 2) is disordered over three sites on a mirror with refined occupancies of 0.480(5), 0.287(7), and 0.234(6). It is assumed that the molecule in its solid state as $[Cu_2^{II}(\mathbf{L})Cl_3]_n{\cdot}nCl{\cdot}xH_2O$ would provide a charge-balanced formula as $[Cu_2^{II}(\mathbf{L})Cl_4]$, (1) in solution which was used for the solution binding studies. The macrocycles are connected through the axial chloride to form an infinite polymeric chain along the *c*-axis, sitting

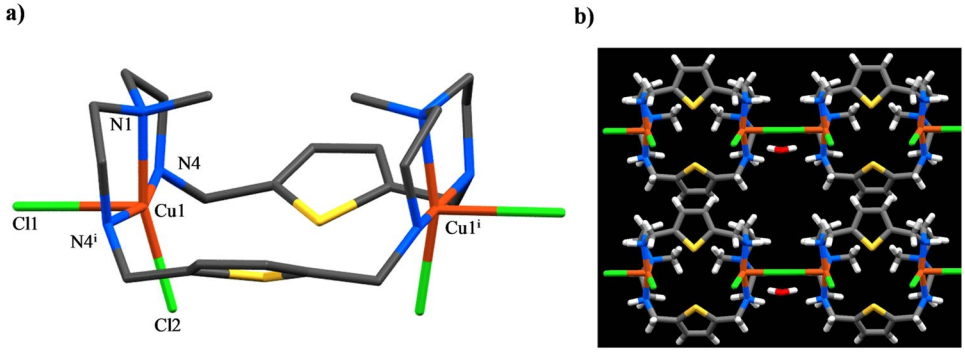

Figure 2. (**a**) Side view of the $[Cu_2^{II}(\mathbf{L})Cl_4]$ motif in the crystal structure of $[Cu_2^{II}(\mathbf{L})Cl_3]_n \cdot nCl \cdot xH_2O$: Hydrogen atoms are not shown for clarity. (**b**) Crystal packing as viewed along the *a*-axis.

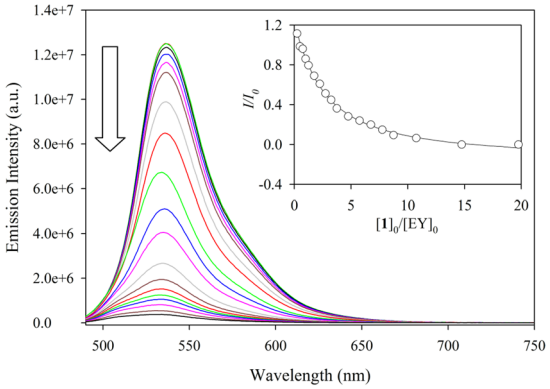

Figure 3. The quenching of fluorescence intensity of EY upon the gradual addition of **1** in water at pH 7.0 [$\lambda_{ex} = 470$ nm, $\lambda_{em} = 536$ nm]. The inset shows the titration plot of I/I_0 against $[\mathbf{1}]_0/[EY]_0$ at $\lambda_{em} = 536$ nm.

on a crystallographic site of *mm* symmetry. Furthermore, each chain is linked with a neighboring chain through the CH···π interactions of two aromatic groups, providing a sheet-like structure (Fig. 2b).

Fluorescence Binding Studies Based on IDA Mechanism. An indicator displacement assay (IDA) was introduced by Anslyn in his elegant work on anion receptors for sensing of citrate in beverages[26,46]. In this case, a negatively charged fluorescent dye (5-carboxyfluorescein) was employed to bind to a receptor consisting of three guanidinium groups, forming an ensemble through charge pairing and/or hydrogen bonding interactions. Upon the addition of citrate, the dye was removed from the ensemble due to the stronger interaction with the receptor, leading to a significant absorption change. Previous studies showed that such a principle can be exploited for dinuclear transition metal complexes to examine their binding selectivities for certain anions through metal-ligand bonding interactions[33,40]. In our study, we applied the IDA mechanism to study the anion binding ability of **1** employing a commercially available external fluorescent dye, eosin Y (EY). As shown in Fig. 3, the fluorescence intensity of EY gradually decreased upon the increasing addition of **1** (2.0×10^{-4} M) to a solution of EY (2.0×10^{-6} M), resulting in an almost complete quenching of the emission. The change in the fluorescence intensity (I/I_o) provided the best fit to a 1:1 binding model[45], yielding a binding constant (K) of $2.51 \times 10^5\,M^{-1}$. Such a quenching is due to the ion-pair formation (**1**·EY) of the negatively-charged dye with the metal complex that quenches the excited state of EY through the electron/energy-transfer process[35]. Hence, the adduct **1**·EY could be used as a "fluorescent OFF-ON" probe for optical as well as visual detection of biologically important anions through the restoration of the fluorescence of EY released to the solution.

The **1**·EY adduct was used as a fluorescence probe for a number of anions, including inorganic halides (fluoride, chloride, bromide, and iodide), oxoanions (nitrate, sulfate, perchlorate, and phosphate), and carboxylates (citrate, oxalate, glutamate, adipate, tartrate, benzoate, and acetate). As shown in Fig. 4, the addition of different anions (5 equiv.) to the **1**·EY ensemble resulted in the highest restoration of the fluorescence for citrate followed by oxalate, glutamate, and phosphate. When other carboxylates such as adipate, tartrate, benzoate, and acetate were added to the solution, only a weak enhancement of the fluorescence intensity was observed, indicating that those anions interact weakly with **1**·EY. This observation implies that the host provided binding sites for selected anions through metal-ligand interactions with varying strength, releasing different amounts of the dye to the solution, as signaled by the fluorescence enhancement. In contrast, the fluorescence of the **1**·EY ensemble was unchanged for other inorganic anions including fluoride, chloride, bromide, iodide, nitrate, sulfate, and

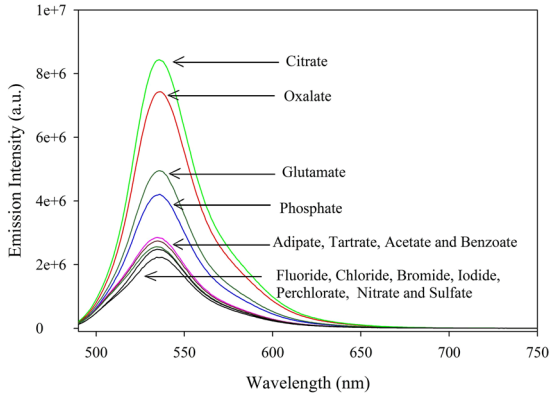

Figure 4. The change in fluorescence intensity of **1**·EY (**1**/EY = 5:1) upon addition of 5 equiv. anions in water at pH 7.0 [$\lambda_{ex} = 470$ nm, $\lambda_{em} = 536$ nm].

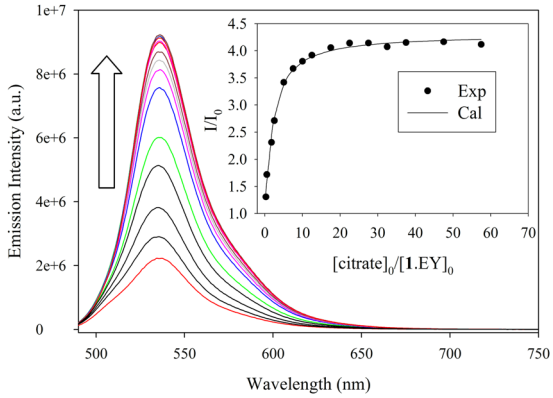

Figure 5. The enhancement of fluorescence intensity of [**1**·EY] (**1**/EY = 5:1, $[EY]_0 = 2.0 \times 10^{-6}$ M) upon the addition of citrate in water at pH 7.0 [$\lambda_{ex} = 470$ nm, $\lambda_{em} = 536$ nm]. The inset shows the titration plot of I/I_0 against $[citrate]_0/[\mathbf{1}\cdot EY]_0$ at $\lambda_{em} = 536$ nm.

perchlorate. This result suggests that the citrate is the strongest candidate among all investigated anions to displace the dye from the dinuclear copper(II) ensemble due to the formation of [**1**·citrate] complex in water.

The binding affinity of **1**·EY for citrate was examined from the titration of **1**·EY with an incremental addition of citrate. Figure 5 shows the gradual enhancement of the fluorescence after the addition of citrate. As determined from the Job's plot, a 1:1 binding was observed (Figure S13 in Supporting Information). Analysis of the binding isotherm from the fitting of I/I_0 with the ratio of $[citrate]_0/[\mathbf{1}\cdot EY]_0$ gave the best fit to a 1:1 binding model[47], providing a conditional binding constant of $K = 6.5 \times 10^5\,M^{-1}$ for the equilibrium of **1**·EY + citrate = **1**·citrate + EY. This value is higher than the binding constant of **1** with EY ($K = 2.51 \times 10^5\,M^{-1}$), making the **1**·EY ensemble ideal for citrate anion. The observed stability for the [**1**·citrate] complex is higher than $7.94 \times 10^4\,M^{-1}$ found for guanidiniocarbonyl pyrroles[27], and comparable to $3.9 \times 10^5\,M^{-1}$ for a cyclam-based Cu(II) complex[48] in water. The conditional binding constants were also determined for other anions including oxalate, glutamate, adipate, tartrate, benzoate, acetate, and phosphate by fluorescence titration experiments of **1**·EY with their potassium salts in water at pH 7.0 under identical conditions, which also provided the best fit for a 1:1 binding of host/guest (Figures S5–S8). The results, as displayed in Table 1, suggest that the new fluorescence probe provides the highest affinity for tribasic citrate among all the anions studied. Other anions including oxalate and glutamate also showed high binding to **1**·EY, with binding constants of 1.9 x.10^5 and 1.0 x.$10^5\,M^{-1}$, respectively. Moderate binding is observed in the case of phosphate and adipate. The **1**·EY ensemble shows the binding affinity for carboxylates in the order of citrate > oxalate > glutamate > adipate > tartrate > acetate > benzoate. However, with the exception for phosphate, no binding is observed for halides and oxoanions to **1**·EY.

The detection limit for citrate was evaluated by titrations of **1**·EY (**1**/EY = 5:1, $[EY]_0 = 2.0 \times 10^{-6}$ M) with an incremental addition of citrate (5.0×10^{-4} M) in water at pH 7. As shown in Fig. 6, the fluorescence ratio (I/I_0) shows a good linear dependency with citrate in the range of 1.25×10^{-6} to 8.60×10^{-6} M ($R^2 = 0.9991$). The linear regression of the fluorescence change provides the equation: $y = 0.1700x + 0.9803$ ($R^2 = 0.9979$), allowing us to estimate the lowest detection limit up to $0.45 \pm 0.02\,\mu M$[49]. A lower detection limit ($0.18 \pm 0.01\,\mu M$) of citrate was recently reported by Yen and coworkers with a thiourea-based cleft; however, it was in a solution of DMSO/H_2O (4/1, v/v)[50].

Anion	K, M^{-1}[a]
Citrate	6.5×10^5
Oxalate	1.9×10^5
Glutamate	1.0×10^5
Phosphate	3.9×10^4
Adipate	1.6×10^4
Tartrate	7.9×10^3
Acetate	1.9×10^3
Benzoate	3.9×10^2

Table 1. Conditional constants (K) for various anions for the equilibria: **1**·EY + Anion = **1**·Anion + EY, as measured by the indicator displacement assay in water at pH 7.0. [a]Estimated deviations are less than 15% (based on the standard deviation from the fit of experimental values).

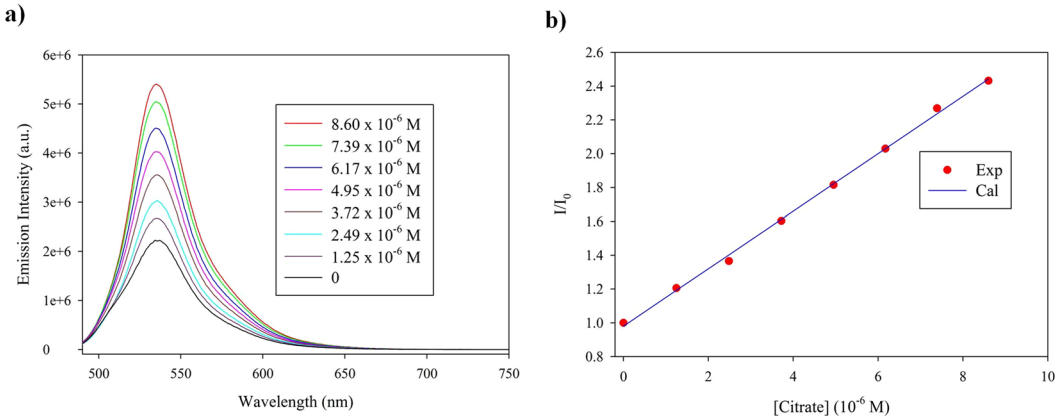

Figure 6. Determination of the detection limit for citrate: (**a**) The enhancement of fluorescence intensity of [**1**·EY] (**1**/EY = 5:1, $[EY]_0 = 2.0 \times 10^{-6}$ M) upon the addition of citrate in the range of 1.25×10^{-6} to $8.60 \times 10^{-6} M^{-1}$; (**b**) Citrate detection scale as plotted with I/I_o against the concentration of citrate [$\lambda_{ex} = 470$ nm, $\lambda_{em} = 536$ nm].

Colorimetric Studies. To evaluate the color-detecting ability of **1**·EY for anions, the ensemble was mixed with 10 equiv. of different anions in water buffered with 20 mM HEPES at pH 7.0, and their colors were examined under both visible and UV light. As shown in Fig. 7, the addition of citrate to **1**·EY resulted in a noticeable color change under visible (top) light as well as under UV light at 365 nm (bottom). Under visible light, the deep magenta color of **1**·EY solution changed to pale orange due to the addition of citrate, tartrate, and phosphate. It is important to note that the color change was very distinct (pale purple to green yellow) for citrate under the UV light at 365 nm, showing almost complete restoration of the original color of EY. For phosphate and tartrate, the color change was still noticeable but with less fluorescence, agreeing with the binding constants measured from fluorescence titrations. Furthermore, the concentration dependent colorimetric titrations, as shown in Fig. 8, suggest that citrate can be detected in water as low as 2 μmol from the color change under the UV light.

Cytotoxicity Assessment. To study the compatibility of **1**·EY as a sensor in a biological system, cytotoxicity was assessed on primary human foreskin fibroblast (HF) cells. These primary cells represent human tissue much better than any commercially available cell line. HF were treated with **1**·EY (0.1– 500 μM) for 72 hours and cell viability was quantified using trypan blue exclusion assay (Figs. 9 and 10)[51]. As shown in Fig. 9, the cell viability was near 100% for up to 100 μM concentration of **1**·EY. However, a significant cell cytotoxicity was observed at higher concentrations of **1**·EY (250 and 500 μM). Taken together, these data indicate excellent biocompatibility of **1**·EY in mammalian cells up to 100 μM concentration.

Computational Studies. To shed additional mechanistic insight into the binding motifs of the dinuclear copper complex, we carried out a series of density functional theory (DFT) calculations using the M06L functional. We have specifically chosen the M06L functional for our studies due to its accuracy and widespread use in various organometallic compounds[52,53] as well as noncovalent interactions for large systems[54]. An all-electron polarized 6–31 g(d, p) basis set was used for all geometry optimizations, and a larger 6–311 g(d, p) basis was used as a final single-point energy on the optimized geometry. Both the geometry optimizations and the final-single point energy calculations were carried out in the presence of a polarizable continuum water model (PCM). The specific PCM model used in this work is the implementation devised by Tomasi and co-workers[55], that creates a solute cavity via a set of overlapping spheres to calculate the solvent reaction field. Fully unconstrained geometry optimizations were carried out on both the isolated receptor as $[Cu_2^{II}(\mathbf{L})Cl_2]^{2+}$ and various citrate-bound motifs.

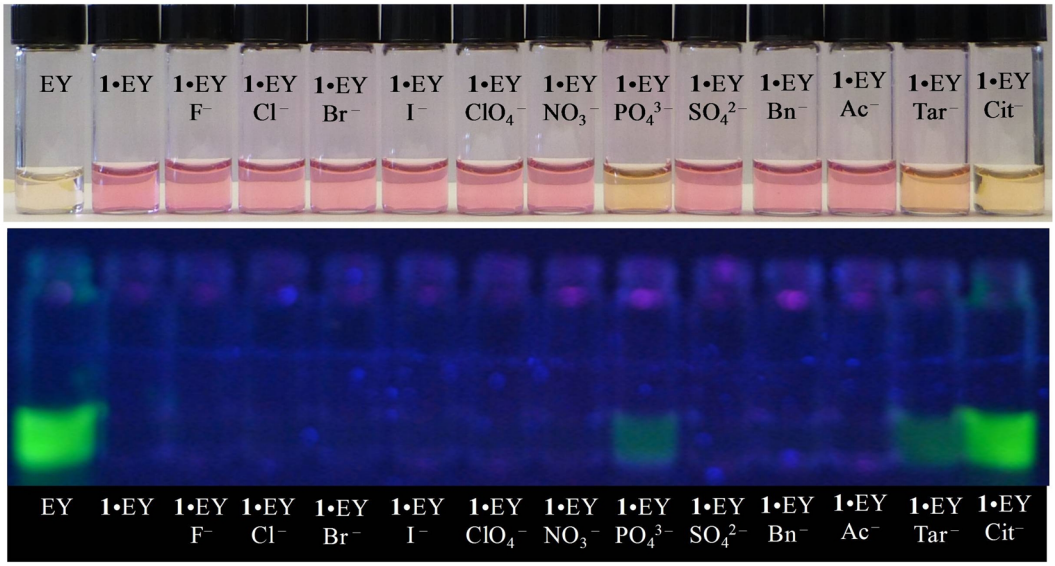

Figure 7. Colorimetric detection of citrate against various anions with **1**·EY (**1**/EY = 5:1, $[EY]_0 = 2 \times 10^{-5}$ M) in water at pH 7.0. Top: visible light; Bottom: UV light at 365 nm. 10 equiv. of anion were added to the solution of **1**·EY.

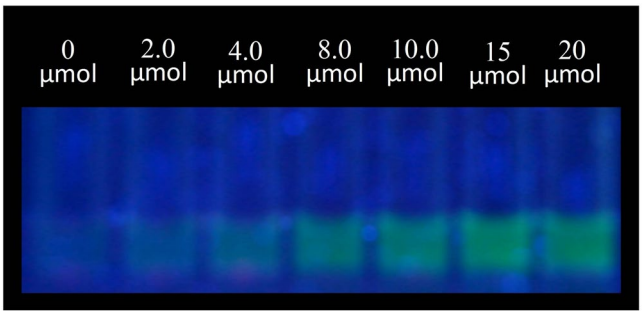

Figure 8. Progressive color change with an increasing amount of citrate in the range of 0 to 20 µmol to [**1**·EY] (**1**/EY = 5:1, $[EY]_0 = 4 \times 10^{-6}$ M) in water at pH 7.0 under UV light at 365 nm.

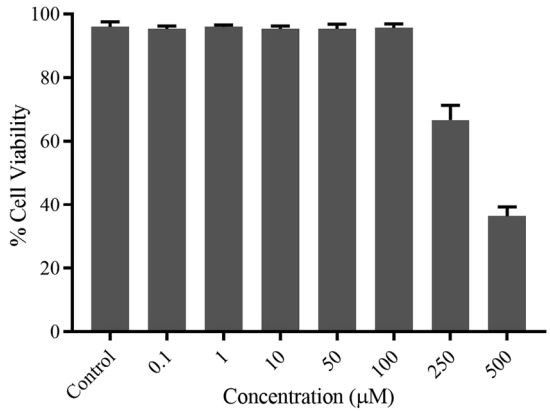

Figure 9. Viability of HF cells upon the treatment with **1**·EY. HF cells were mock treated (control) or treated with **1**·EY (0.1–500 µM) for 72 hours and cell viability was quantified using trypan blue exclusion assay. Error bars represent standard error of the mean from three independent experiments.

From these calculations, we found that the receptor formed a 1:1 complex with citrate, showing two different binding configurations: one with two symmetric carboxylate groups (mode A) and the other with two unsymmetric carboxylate groups (mode B), as shown in Fig. 11. The third unbound carboxylate group in each binding mode

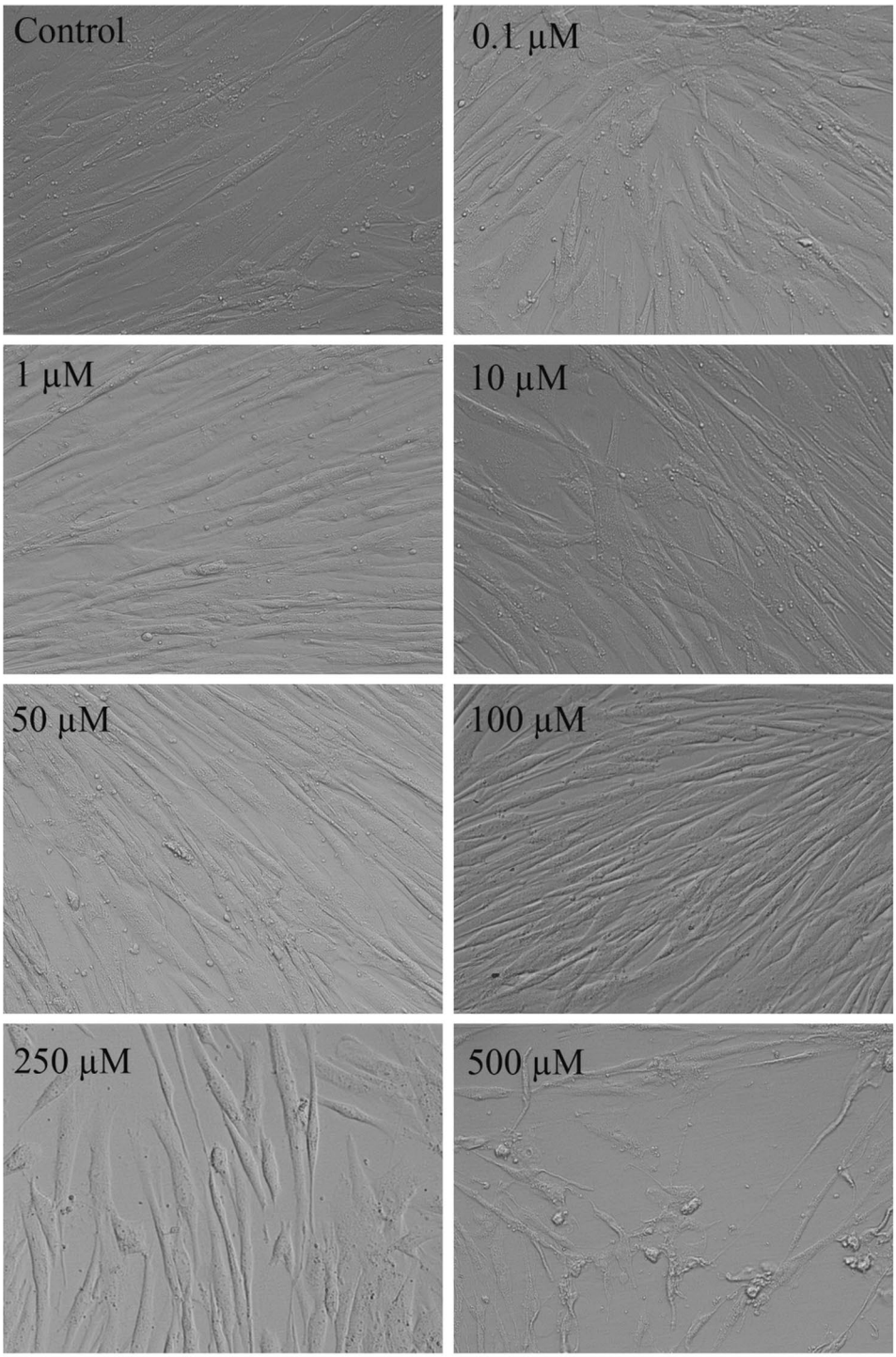

Figure 10. Bright-field images of HF cells upon the treatment with **1**·EY. HF cells were mock treated (control) or treated with **1**·EY (0.1–500 μM) for 72 hours and live cell images were captured.

is H-bonded with the OH group of the citrate (OH···O = 2.533 and 2.620 Å in A and B modes, respectively). For each of the optimized geometries, the binding energy (ΔE) was calculated with a 6–311 g(d, p) basis as described earlier[41], yielding an attractive ΔE of −70.79 kcal/mol for mode A and −73.07 kcal/mol for mode B. The most attractive binding energy for mode B reflects the preferred orientation of the citrate with the dinuclear copper complex in mode B.

Conclusions

A macrocycle-based dinuclear foldamer has been used as an efficient probe in an approach of *Indicator Displacement Assay* for colorimetric and fluorescent sensing of citrate, which operates by a non-covalent binding

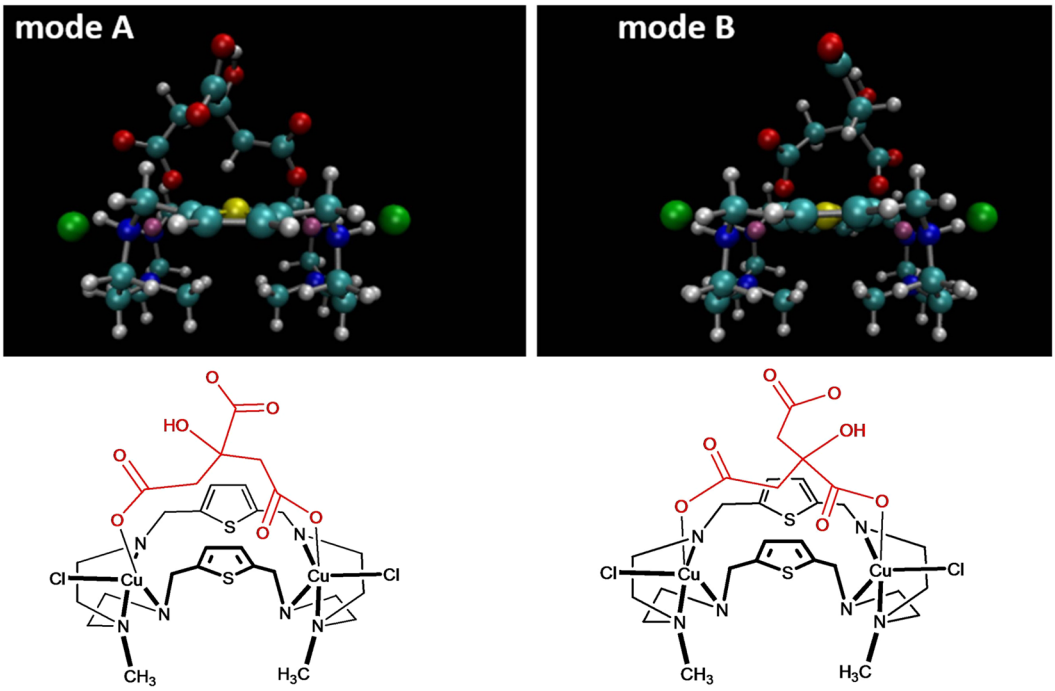

Figure 11. DFT-optimized geometries for two different binding configurations (represented by the chemical structures), denoted as mode A (left) and mode B (right), of the citrate complex with $[Cu_2^{II}(\mathbf{L})Cl_2]^{2+}$ carried out at the M06L/6-31 g(d,p) level of theory.

principle involving metal-ligand interactions in pure water at neutral pH. The addition of citrate to the ensemble led to the complete restoration of the fluorescence (fluorescent-ON) of the dye due to the formation of the complex that was also supported by high level DFT calculations. This readily obtainable chemosensor has been shown to recognize citrate with strong sensitivity and selectivity over a wide range of anions in water, displaying a detectable color change under both visible and UV light in water up to 2 μmol. The synthesized ensemble is capable of sensing a citrate anion with the lowest detection limit up to 0.45 ± 0.02 μM in water, as calculated from the emission change. The dinuclear complex has been proven to be fully biocompatible in human foreskin fibroblast cells. The excellent anion binding properties in water and biocompatibility observed towards mammalian cells demonstrates that this chemosensor can be used as a potential sensing probe for the detection of biologically relevant citrate anions for various biological and chemical applications.

Methods

General. The chemicals used for this work were purchased from Sigma-Aldrich as reagent grade and used as received. Nuclear magnetic resonance (NMR) spectra were recorded at 25 °C on a Varian Unity INOVA 500 FT-NMR. Chemical shifts were measured in $CDCl_3$ and calibrated against TMS as an external reference used in a sealed capillary tube. All NMR data were processed and analyzed with MestReNova Version 6.1.1-6384. The mass spectral data were obtained using an ESI-MS positive mode on a FINNIGAN LCQDUO. Elemental analysis was carried out using an ECS 4010 Analytical Platform (Costech Instrument) at Jackson State University. The fluorescence titrations were carried out using a Fluoromax-4 spectrofluorometer (HORIBA Scientific).

Synthesis. ***L****: N*-methyl-2,2′-diaminodiethylamine (0.6042 g, 5.1×10^{-3} mol) in CH_3OH (300 mL) and 2,5-thiophenedicarboxyaldehyde (0.7218 g, 5.1×10^{-3} mol) in CH_3OH (300 mL) were added simultaneously to a three-neck flask containing 600 mL of CH_3OH over 4 h under stirring at 0 °C. The reaction mixture was further stirred overnight at room temperature. The solvent was removed under vacuum, and 100 mL of CH_3OH was added to the residue. The imine that formed was reduced by $NaBH_4$ (1.2 g) at room temperature overnight. The solvent was removed under vacuum, and the resulting reaction product was dispersed in water (100 mL). The aqueous phase was extracted by CH_2Cl_2 (3×100 mL). The organic portions were collected and dried by anhydrous $MgSO_4$ (2g). The solid was filtered off, and the solvent was evaporated to dryness. The crude product was purified by column chromatography (neutral alumina, 2% CH_3OH in CH_2Cl_2). Yield: 0.82 g, (62%). ^{1}H NMR (500 MHz, $CDCl_3$, TMS): δ 6.75 (s, 4 H, Ar*H*), 3.91 (s, 8 H, ArCH_2), 2.71 (t, 8 H, $J = 5.5$ Hz, NCH_2CH_2), 2.48 (t, 8 H, $J = 5.5$ Hz, NCH_2CH_2), 2.14 (s, 6 H, NCH_3), ^{13}C NMR (125 MHz, $CDCl_3$): δ 124.48 (Ar-C), 56.70 (ArCH_2), 48.64 (NCH_2CH_2), 46.28 (NCH_2CH_2), 42.32 (NCH_3). ESI-MS: m/z (+) 451.3 $[M+H]^+$. Anal. Calcd. for $C_{22}H_{36}N_6S_2$: C, 58.63; H, 8.50; N, 18.65. Found: C, 58.60; H, 8.52; N, 18.48.

*$[Cu_2^{II}(\mathbf{L})Cl_4]\cdot H_2O$, (**1**).* The free amine **L** (100 mg, 0.222 mmol) was mixed with two equiv. of $CuCl_2\cdot H_2O$ (75.7 mg, 0.444 mmol) in 2 mL of H_2O. The solution was stirred at 60 °C for one hour. The deep blue solid that

appeared immediately was collected by filtration and washed by diethyl ether. The microcystals were recrystallized from slow evaporation of a water solution, yielding X-ray quality crystals. Yield: 150 mg, 88% yield. The compound was characterized by X-ray diffractometer. Anal. Calcd. for $C_{22}H_{38}Cl_4Cu_2N_6OS_2$: C, 35.92; H, 5.21, N, 11.42. Found: C, 35.85; H, 5.22; N, 11.44.

Fluorescence Titration Studies. All fluorescence titrations were performed using a Fluoromax-4 spectrofluorometer (HORIBA Scientific) in water at pH 7.0. The pH was adjusted by using 0.02 M HEPES purchased from Sigma Aldrich Chemical Company. The experimental conditions were used as: $\lambda_{ex} = 470$ nm, $\lambda_{em} = 536$ nm, $d_{ex} = 2$, $d_{em} = 5$ for eosin Y dye.

*Binding constant of **1** for EY.* The binding affinity of **1** for EY for the formation of **1**·EY was determined from the titration of EY with **1** in water at pH 7.0. In this case, the quenching of fluorescence was observed after the addition of **1** to EY. Initial concentrations of EY and **1** were 2.0×10^{-6} M and 2.0×10^{-4} M, respectively. Each titration was performed by 15 measurements varying the $[\mathbf{1}]_0/[\text{dye}]_0 = 0$–25, and the association constant (K) was calculated by fitting the ratio of I/I_0 with a 1:1 association model using eq. (1).

$$\Delta\Phi = ([\mathbf{1}]_0 + [\text{EY}]_0 + 1/K - ([\mathbf{1}]_0 + [\text{EY}]_0 + 1/K)^2 - 4[\text{EY}]_0[\mathbf{1}]_0)_{1/2})\Delta\Phi_{max}/2[\text{EY}]_0 \quad (1)$$

where $\Phi = I/I_0$, I_0 = initial fluorescence intensity of EY, I = fluorescence intensity after the addition of **1**. The error limit in K was less than 15%.

*Conditional constants of **1**·EY for anions.* The binding affinity of **1**·EY for different anions was examined from the competition reaction, and the conditional constants were derived from the titration of **1**·EY with anions in water under the same experimental conditions described in the preceding section. In this case, EY was displaced by the addition of an anion, resulting in an enhancement of the fluorescence intensity. Initial concentrations of **1**·EY (**1**/EY = 5:1) and an anion were 2.0×10^{-6} M, and 2.0×10^{-3} M, respectively. Each titration was performed by 15 measurements varying the $[\text{anion}]_0/[\mathbf{1}\cdot\text{EY}]_0 = 0$–60, and the conditional constant (K) was calculated by fitting the ratio of I/I_0 with a 1:1 association model using eq. (2).

$$\Delta\Phi = ([\text{A}]_0 + [\mathbf{1}\cdot\text{EY}]_0 + 1/K - ([\text{A}]_0 + [\mathbf{1}\cdot\text{EY}]_0 + 1/K)^2 - 4[\mathbf{1}\cdot\text{EY}]_0[\text{A}]_0)_{1/2})\Delta\Phi_{max}/2[\mathbf{1}\cdot\text{EY}]_0 \quad (2)$$

where, $\Phi = I/I_0$, A = anion, I_0 = initial fluorescence intensity of **1**·EY, I = fluorescence intensity after the addition of an anion. The error limit in K was less than 15%.

Colorimetric studies. The colorimetric studies of the **1**·EY ensemble for different anions were performed under both visible and UV light (365 nm). Stock solutions of $[\mathbf{1}] = 2 \times 10^{-3}$ M, $[\text{EY}] = 2 \times 10^{-3}$ M and $[\text{anion}] = 2 \times 10^{-3}$ M were prepared separately in water buffered with a 0.02 M HEPES solution at pH = 7.0. The **1**·EY ensemble was prepared by mixing **1** with EY at a ratio of 5:1. The **1**·EY ensemble was mixed with 10 equiv. of each anion, and the solution was further diluted to maintain the concentration of $[\text{EY}] = 2 \times 10^{-5}$ M. Each sample (1 mL) was transferred in a vial and the color was examined by naked eye under both a visible light and a UV lamp at 365 nm.

The colorimetric detection limit of citrate was evaluated using a 0.02 M HEPES solution in water at pH = 7.0. The stock solutions of **1** (2×10^{-3} M) was mixed with EY (2×10^{-3} M) at a ratio of 5:1 and the solution was further diluted to maintain a concentration of $[\text{EY}] = 4 \times 10^{-6}$ M. A stock solution of $[\text{citrate}] = 2 \times 10^{-3}$ M was prepared in water buffered with a 0.02 M HEPES solution. 0, 1.0, 2.0, 4.0, 5.0, 7.5, and 10.0 µL of citrate (2×10^{-3} M) were added separately to a vial containing 1.0 mL of **1**·EY ($[\mathbf{1}]/[\text{EY}] = 5{:}1$, $[\text{EY}] = 4 \times 10^{-6}$ M). Final concentrations of the citrate solution were 0, 2.0, 4.0, 8.0, 10.0, 15.0, and 20 µM. The samples were then examined under both visible and UV light.

X-ray Crystallography. Intensity data for **1′** were collected using a diffractometer with a Bruker APEX ccd area detector[56] and graphite-monochromated MoKα radiation (λ = 0.71073 Å). The sample was cooled to 100(2) K. Cell parameters were determined from a non-linear least squares fit of 5856 peaks in the range $2.42 < \theta < 28.25$. The orthorhombic space group *Amm*2 was determined by systematic absences and statistical tests and verified by subsequent refinement. The structure was solved by direct methods and refined by full-matrix least-squares methods on F^2[57]. The absolute structure was determined by refinement of the Flack parameter[58]. The polar axis restraints were taken from Flack and Schwarzenbach[59]. Crystal data: $[Cu_2^{II}(C_{22}H_{36}N_6S_2)Cl_3]_n \cdot nCl \cdot xH_2O$, orthorhombic, $a = 11.7449(10)$ Å, $b = 16.8588(14)$ Å, $c = 8.0948(7)$ Å, $\alpha = 90°$, $V = 1602.8(2)$ Å^3, $T = 100(2)$ K, space group *Amm*2, $Z = 2$, 14889 reflections measured, 2152 independent reflections, $R_{int} = 0.0344$, $R_1 = 0.0279$ (all data). CCDC 1017159.

Cytotoxicity Assessment. Primary human foreskin-derived fibroblasts (HF) were cultured in Dulbecco's modified Eagle's medium (DMEM) (Cellgro, Manassas, VA) containing 4.5 g/ml glucose, 10% fetal bovine serum (SAFC, Lenexa, KS), 1 mM sodium pyruvate, 2 mM L-glutamine, and 100 U/ml penicillin-streptomycin (Cellgro) at 37 °C with 5% CO_2[60]. HF cells were seeded in 12-well plates and allowed for 24 hours for confluency before treatment with **1**·EY at a final concentration from 0.1–500 µM. At 72 hours post treatment, bright-field images of living cells were captured using an inverted Evos-FL microscope (Thermo Fisher Scientific, Waltham, MA). After imaging, cell viability was determined by a trypan blue exclusion assay[51] as previously described[61] using a TC20 automated cell counter (Bio-Rad Laboratories, Hercules, CA). In brief, cells were harvested using 0.025% Trypsin-EDTA (Gibco, Thermo Fisher Scientific) diluted in phosphate-buffered saline and neutralized with equal volume of supplemented DMEM. 10 µl of cell suspension was mixed with an equal volume of trypan blue

(Hyclone Laboratories, Logan, UT) and 10 µl of mixture was loaded immediately into the outer chamber of the counting slide. The slide was inserted into the slide slot of the cell counter, and percent of viable cells was calculated automatically.

Computational Methods. All quantum chemical calculations in this study utilized the Gaussian 09 package[62].

Data Availability. All data generated or analyzed during this study are included in this published article and its Supplementary Information files.

References

1. Evans, N. H. & Beer, P. D. Advances in Anion Supramolecular Chemistry: From Recognition to Chemical Applications. *Angew. Chem. Int. Ed.* **53**, 11716–11754 (2014).
2. Cametti, M. & Rissanen, K. Recognition and sensing of fluoride anion. *Chem. Commun.* **20**, 2809–2829 (2009).
3. Madhuprasad, Bhat, M., P., Jung, H.-Y., Losic, D. & Kurkuri, M. D. anion sensors as logic gates: A close encounter? *Chem. Eur. J.* **22**, 6148–6178 (2006).
4. Gale, P. A., Howe, E. N. W. & Wu, X. Anion receptor chemistry. *Chem.* **1**, 351–422 (2016).
5. Langton, M. J., Serpell, C. J. & Beer, P. D. Anion recognition in water: Recent advances from a supramolecular and macromolecular perspective. *Angew. Chem., Int. Ed.* **55**, 1974–1987 (2016).
6. Hossain, M. A. Inclusion complexes of halide anions with macrocyclic receptors. *Curr. Org. Chem.* **12**, 1231–1256 (2008).
7. Khansari, M. E. *et al*. Remarkable hexafunctional anion receptor with operational urea-based *inner cleft* and thiourea-based *outer cleft*: Novel design with high-efficiency for sulfate binding. *Sci. Rep.* **7**, 6032 (2017).
8. Liu, S.-Y. *et al*. Cholic-acid-based fluorescent sensor for dicarboxylates and acidic amino acids in aqueous solutions. *Org. Lett.* **7**, 5825–5828 (2005).
9. Kacprzak, K. & Gawronski, J. Bifunctional receptor triad for efficient recognition of mono-and dicarboxylic acids. *Chem. Commun.* **13**, 1532–1533 (2003).
10. Linton, B. R., Goodman, M. S., Fan, E., van Arman, S. A. & Hamilton, A. D. Thermodynamic aspects of dicarboxylate recognition by simple artificial receptors. *J. Org. Chem.* **66**, 7313–7319 (2001).
11. Krebs, H. A. & Weitzman, P. D. J. *Krebs' citric acid cycle: half a century and still turning*, London: Biochemical Society (1987).
12. Pal, R., Parker, D. & Costello, L. C. A europium luminescence assay of lactate and citrate in biological fluids. *Org. Biomol. Chem.* **7**, 1525–1528 (2009).
13. Robertson, W. G. & Hughes, H. Importance of mild hyperoxaluria in the pathogenesis of urolithiasis–new evidence from studies in the Arabian peninsula. *Scanning Microsc.* **7**, 391–401 (1993).
14. Marengo, S. R. & Romani, A. M. P. Oxalate in renal stone disease: the terminal metabolite that just won't go away. *Nat Clin Pract Nephrol.* **4**, 368–377 (2008).
15. Palsson, R. & Niles, J. L. Regional citrate anticoagulation in continuous venovenous hemofiltration in critically ill patients with a high risk of bleeding. *Kidney International.* **55**, 1991–1997 (1999).
16. Kale, P. N. & Adsule, P. G. *Handbook of Fruit Science and Technology: Product-rim, Composition, Storage, and Processing* (Eds: Salunke, D. K.; Kadam, S. S.; Marcel Dekker, New York, 1995, Ch. 3).
17. Cebotaru, V. *et al*. High citrate diet delays progression of renal insufficiency in the ClC-5 knockout mouse model of Dent's disease. *Kidney Int.* **68**, 642–652 (2005).
18. Schell-Feith, E. A. *et al*. Does citrate prevent nephrocalcinosis in preterm neonates? *Pediatr. Nephrol.* **21**, 1830–1836 (2006).
19. DeBorba, B. M., Rohrer, J. S. & Bhattacharyya, L. Development and validation of an assay for citric acid/citrate and phosphate in pharmaceutical dosage forms using ion chromatography with suppressed conductivity detection. *J. Pharm. Biomed. Anal.* **36**, 517–524 (2004).
20. Ribeiro, C. M. F., Matos, C. D., Sales, M. G. F. & Vaz, M. C. V. F. Citrate selective electrodes for the flow injection analysis of soft drinks, beers and pharmaceutical products. *Anal. Chim. Acta.* **471**, 41–47 (2002).
21. Lynch, M. L. & Nicholson, J. K. Proton MRS of human prostatic fluid: Correlations between citrate, spermine, and myo-inositol levels and changes with disease. *Prostat* **30**, 248–255 (1997).
22. Kim, S. K., Lee, D. H., Hong, J.-I. & Yoon, J. Chemosensors for Pyrophosphate. *Chem. Soc. Res.* **42**, 23–31 (2009).
23. Schmuck, C. & Schwegmann, M. A naked-eye sensing ensemble for the selective detection of citrate but not tartrate or malate in water based on a tris-cationic receptor. *Org. Biomol. Chem.* **4**, 836–838 (2006).
24. Mateus, P., Delgado, R., Brandão, P. & Félix, V. Dicarboxylate Recognition by Two Macrobicyclic Receptors: Selectivity for Fumarate over Maleate. *J. Org. Chem.* **77**, 4611–4621 (2012).
25. Ghosh, K. & Sarkar, A. R. Pyridinium-based symmetrical diamides as chemosensors in visual sensing of citrate through indicator displacement assay (IDA) and gel formation. *Org. Biomol. Chem.* **9**, 6551–6558 (2011).
26. Metzger, A. & Anslyn, E. V. A chemosensor for citrate in beverages. *Angew. Chem., Int. Ed. Engl.* **37**, 649–652 (1998).
27. Schmuck, C. & Schwegmann, M. A molecular flytrap for the selective binding of citrate and other tricarboxylates in water. *J. Am. Chem. Soc.* **127**, 3373–3379 (2005).
28. Mishra, A. *et al*. Self-assembled metalla-bowls for selective sensing of multi-carboxylate anions. *Dalton Trans.* **41**, 1195–1201 (2012).
29. Fabbrizzi, L. & Poggi, A. Anion recognition by coordinative interactions: metal–amine complexes as receptors. *Chem. Soc. Rev.* **42**, 1681–1699 (2013).
30. Mateus, P., Lima, L. M. P. & Delgado, R. Di-and trinuclear copper(II) complexes of polyaza macrocycles and cryptands as anion receptors. *Polyhedron* **52**, 25–42 (2013).
31. Harding, C. J., Mabbs, F. E., MacInnes, E. J. L., McKee, V. & Nelson, J. Cascade complexation of pseudo-halide by dicopper cryptates: a linear Cu–NNN–Cu unit. *J. Chem. Soc., Dalton Trans.* **15**, 3227–3230 (1996).
32. Amendola, V. *et al*. Halide-Ion Encapsulation by a Flexible Dicopper (II) Bis-Tren Cryptate. *Angew. Chem., Int. Ed.* **112**, 3039–3042 (2000).
33. Amendola, V., Bergamaschi, G., Buttafava, A., Fabbrizzi, L. & Monzani, E. Recognition and sensing of nucleoside monophosphates by a dicopper (II) cryptate. *J. Am. Chem. Soc.* **132**, 147–156 (2010).
34. Chen, J. M. *et al*. Anion recognition of chloride and bromide by a rigid dicobalt (II) cryptate. *Inorg. Chem.* **47**, 3158–3165 (2008).
35. De Santis, G., Fabbrizzi, L., Licchelli, M., Poggi, A. & Taglietti, A. Molecular recognition of carboxylate ions based on the metal–ligand interaction and signaled through fluorescence quenching. *Angew. Chem., Int. Ed. Engl.* **35**, 202–204 (1996).
36. Carvalho, S., Delgado, R., Drew, M. G. B. & Félix, V. Dicopper (II) complexes of a new di-para-xylyldioxatetraazamacrocycle and cascade species with dicarboxylate anions: thermodynamics and structural properties. *Dalton Trans.* **23**, 2431–2439 (2007).
37. Rhaman, M. M., Powell, D. R. & Hossain, M. A. Supramolecular assembly of uridine monophosphate (UMP) and thymidine monophosphate (TMP) with a dinuclear copper(II) receptor. *ACS Omega* **2**, 7803–7811 (2017).
38. Li, F., Delgado, R. & Félix, V. Hexaazamacrocycle containing pyridine and its dicopper complex as receptors for dicarboxylate anions. *Eur. J. Inorg. Chem.* **22**, 4550–4561 (2005).

39. Mendy, J. S., Saeed, M. A., Fronczek, F. R., Powell, D. R. & Hossain, M. A. Anion recognition and sensing by a new macrocyclic dinuclear copper (II) complex. *Inorg. Chem.* **49**, 7223–7225 (2010).
40. Saeed, M. A., Powell, D. R. & Hossain, M. A. Fluorescent detection of phosphate anion by a highly selective chemosensor in water. *Tetrahedron Lett.* **51**, 4904–4907 (2010).
41. Rhaman, M. M., Alamgir, A., Wong, B. M., Powell, D. R. & Hossain, M. A. A highly efficient dinuclear Cu(II) chemosensor for colorimetric and fluorescent detection of cyanide in water. *RSC Advances* **4**, 54263–54267 (2014).
42. Rhaman, M. M., Fronczek, F. R., Powell, D. R. & Hossain, M. A. Colourimetric and fluorescent detection of oxalate in water by a new macrocycle-based dinuclear nickel complex: a remarkable red shift of the fluorescence band. *Dalton Trans.* **43**, 4618–4621 (2014).
43. Motekaitis, R. J., Martell, A. E., Dietrich, B. & Lehn, J.-M. Anion binding in macrobicyclic metal cryptate complexes: copper(II)-BISTREN. *Inorg. Chem.* **23**, 1588–1591 (1984).
44. Tang, L.-J. *et al.* Tight binding and fluorescent sensing of oxalate in water. *J. Am. Chem. Soc.* **130**, 12606–12607 (2008).
45. Rhaman, M. M. *et al.* Encapsulation and selectivity of sulfate with a furan-based hexaazamacrocyclic receptor in water. *Org. Biomol. Chem.* **12**, 2045–2048 (2014).
46. Metzger, A., Lynch, V. M. & Anslyn, E. V. A synthetic receptor selective for citrate. *Angew. Chem., Int. Ed. Engl.* **36**, 862–865 (1997).
47. Schneider, H. J., Kramer, R., Simova, S. & Schneider, U. Host-guest chemistry. Solvent and salt effects on binding constants of organic substrates in macrocyclic host compounds. *A general equation measuring hydrophobic binding contributions. J. Am. Chem. Soc.* **110**, 6442–6448 (1998).
48. Fabbrizzi, L., Foti, F. & Taglietti, A. Metal-containing trifurcate receptor that recognizes and senses citrate in water. *Org. Lett.* **7**, 2603–2606 (2005).
49. Ono, A. & Togashi, H. Highly selective oligonucleotide-based sensor for mercury (II) in aqueous solutions. *Angew. Chem. Int. Ed.* **43**, 4300–4302 (2004).
50. Liu, Z.-H., Devaraj, S., Yang, C.-R. & Yen, Y.-Pin A new selective chromogenic and fluorogenic sensor for citrate ion. *Sensors Actuators B.* **174**, 555–562 (2012).
51. Strober, W. Trypan blue exclusion test of cell viability. *Curr. Protoc. Immunol*, Appendix 3:Appendix3B (2001).
52. Haque, S. A., Bolhofner, R. L., Wong, B. M. & Hossain, M. A. Colorimetric and optical discrimination of halides by a simple chemosensor. *RSC Advances* **5**, 38733–38741 (2015).
53. Gusev, D. G. Assessing the accuracy of M06-L organometallic thermochemistry. *Organometallics* **32**, 4239–4243 (2013).
54. Huang, C. *et al.* Spectroscopic properties of nanotube–chromophore hybrids. *ACS Nano* **5**, 7767–7774 (2011).
55. Fortenlli, A. & Tomasi, J. The implementation of density functional theory within the polarizable continuum model for solvation. *Chem. Phys. Lett.* **231**, 34–39 (1994).
56. Bruker, SADABS. Bruker AXS Inc., Madison, Wisconsin, USA (2002).
57. Sheldrick, G. M. SHELXL University of Gottingen (2013).
58. Parsons, S. & Flack, H. D. Precise absolute-structure determination in light-atom crystals. *Acta Cryst.A* **60**, S61 (2004).
59. Flack, H. D. & Schwarzenbach, D. On the use of least-squares restraints for origin fixing in polar space groups. *Acta Cryst. A* **44**, 499–506 (1988).
60. Freshney, R. I. Culture of Animal Cells: A Manual of Basic Technique, 5th edition. New York: Wiley Liss (2005).
61. Archer, M. A. *et al.* Inhibition of endocytic pathways impacts cytomegalovirus maturation. *Sci. Rep.* **7**, 46069 (2017).
62. Frisch, M. J. *et al. Gaussian 09, Revision D.01*, Gaussian, Inc.: Wallingford CT (2009).

Acknowledgements

This work was supported by the National Institutes of Health (G12RR013459). M.H.H. and R.T. are supported by American Heart Association (Award No. 14SDG20390009). All DFT calculations by L. X. and B. M. W. were supported by the U.S. Department of Energy, Office of Science, Early Career Research Program under Award No. DE-SC0016269. The diffractometer was paid for in part by the National Science Foundation (grant CHE-0130835).

Author Contributions

M.M.R. and A.A. carried out the synthesis, titrations and colorimetric studies. M.H.H. and R.T. performed cytotoxicity assessments. L.X. and B.M.W. conducted computational studies. D.R.P. solved the crystal structure. M.A.H. designed the experiments and wrote the manuscript. All authors revised the manuscript.

Additional Information

Supplementary information accompanies this paper at https://doi.org/10.1038/s41598-017-18322-w.

Competing Interests: The authors declare that they have no competing interests.

Publisher's note: Springer Nature remains neutral with regard to jurisdictional claims in published maps and institutional affiliations.